fibers

MDPI

Article

Durability of Recycled Steel Fiber Reinforced Concrete in Chloride Environment

Cristina M. V. Frazão [1,*], Joaquim A. B. Barros [2] and J. Alexandre Bogas [3]

[1] ISISE, Department of Civil Engineering, University of Minho, Campus de Azurém, 4800-058 Guimarães, Portugal
[2] ISISE, Department of Civil Engineering, University of Minho, Campus de Azurém, 4800-058 Guimarães, Portugal; barros@civil.uminho.pt
[3] ICIST, Department of Civil Engineering and Architecture, Technical University of Lisbon, 1649-004 Lisbon, Portugal; abogas@civil.ist.utl.pt
* Correspondence: cristina.frazao@civil.uminho.pt

Received: 30 September 2019; Accepted: 9 December 2019; Published: 16 December 2019

Abstract: For structural elements exposed to chloride environments, an important aspect of Recycled Steel Fiber Reinforced Concrete (RSFRC) durability is the corrosion resistance. In the present work, an experimental program was carried out to evaluate the long-term effects of chloride attack on the post-cracking behavior of RSFRC by performing splitting tensile tests and round panel tests. Two RSFRC mixtures defined based on the packing density optimization were produced with a fiber content of 0.8% and 1% per volume of concrete. The influence of different periods of chloride immersion was investigated, as well as the influence of fiber dispersion at crack surfaces of the specimens. Additionally, a simplified prediction of the long-term chloride penetration depth into uncracked RSFRC under immersion aggressive chloride exposure conditions was estimated. The RSFRC revealed high susceptibility to surface corrosion under the chloride exposure conditions adopted. However, the post-cracking resistance of RSFRC was not significant affected. The addition of RSF had a negligible effect in the diffusion of chloride ions into concrete, and the critical chloride content was higher than that found in conventional reinforced concrete structures.

Keywords: recycled steel fiber reinforced concrete (RSFRC); post-cracking behavior; durability; chloride attack; splitting tensile test; round panel test

1. Introduction

Chloride-induced reinforcement corrosion has been reported to be the leading cause of degradation of reinforced concrete (RC) structures exposed in coastal/marine environments [1,2]. In environments containing chlorides, Steel Fiber Reinforced Concrete (SFRC) structures are subjected to chloride attack that can promote the depassivation and subsequent corrosion of steel fibers, with eventual pernicious consequences in terms of structural and durability performance.

Corrosive agents may penetrate the concrete through one of the four main transport mechanisms: Diffusion, Capillary Suction, Permeation, and Migration [3]. The chloride penetration into uncracked concrete depends of the SFRC pore structure and all the mix design parameters that determine it, such as water-to-cement (w/c) ratio, type and proportion of mineral admixtures and cement, type and content of steel fibers, compaction, and curing. The concrete permeability may decrease significantly with the addition of fibers due to the reduction of shrinkage cracks and the breaking of pore continuity by the fiber reinforcement mechanisms [4].

The main variables affecting the durability of uncracked SFRC exposed to chlorides are the exposure conditions, type and size of the steel fibers, and the quality of the concrete matrix [5].

However, in general, it is reported that the durability of uncracked concrete is little affected with the addition of steel fibers [6–8].

The steel fibers are protected by the high alkalinity (pH > 13.5) of the pore solution of concrete that causes the formation of a protective oxide film on the steel fibers surface, passivating them [9]. This film can be destroyed when the chloride ions penetrate the SFRC and exceed the critical threshold chloride content [9]. This critical chloride content depends on various factors, such as, oxygen concentration, binder type, w/c ratio, steel grade and test conditions [10], and has been found to be much higher in steel fibers than in conventional reinforcing steel, which may ensure larger service life of SFRC structures in chloride environment [11–13]. According to [11], the improved corrosion resistance of steel fibers in uncracked concrete can be attributed to the combination of two factors: the short length of the steel fibers that impedes large potential differences along the fiber; the casting conditions that allow the formation of a very thin well-defined cement paste-steel interfacial layer rich in $Ca(OH)_2$ with less presence of voids at the interface. However, some authors have reported the opposite, i.e., a higher rate of chloride transport in SFRC compared to plain concrete, due to the increased porosity at the interface of steel fibers/matrix, caused by the air bubbles arrested by the fibers during the casting process [12]. Nevertheless, in environments containing chlorides, it has been reported that only steel fibers near the concrete surface are susceptible to corrosion, which has only an aesthetic detrimental impact [14].

The estimation of service lifetime of existing and new reinforced concrete (RC)-based constructions is very important for planning future maintenance and repair of the structures. Different models for service life predictions of the chloride ingress in RC structures exposed to marine environment, have been proposed by several researchers [15–18], essentially based on the application of the Fick's 2nd law of diffusion during the corrosion initiation period. However, few studies in this regard are available for SFRC.

Recycled Steel Fibers (RSF) derived from the tire recycling industry can be an effective reinforcement for structural and non-structural concrete applications with beneficial economic and environmental impact. As reported in the literature [19–25], RSF have been successfully used in concrete to improve its post-cracking load bearing capacity and energy absorption performance, and also to limit the crack width, with beneficial consequences in terms of concrete durability. The heterogeneity of each RSF regarding the geometry and microstructure provides a plurality of strengthening mechanisms to concrete that promotes efficiency and durability, as long as the Recycled Steel Fiber Reinforced Concrete (RSFRC) composition is carefully adjusted to the presence of RSF. RSF reinforcement can significantly reduce the brittle behavior of concrete by improving its toughness and post-cracking resistance [20,22,23,26]. RSF are also used in concrete to restrain the crack opening by bridging the crack surfaces, which leads to improved post-cracking load bearing and energy absorption capacity, with beneficial consequences in terms of concrete durability [21,27,28]. However, this ability of the RSF to transfer stresses through a cracked section depends on the effectiveness of the fiber reinforcement, i.e., fiber properties and fiber orientation and distribution [29]. In this sense, these effects should be considered for structural design, since variations of fiber dispersion may affect the mechanical properties [30].

The fiber reinforcement efficiency in improving the post-cracking load bearing capacity and energy absorption performance of concrete can be assessed by splitting tensile tests governed by a localized crack. However, for slab and shell type structures, the design methodology should be based on constitutive laws, for example, derived from FRC panel with cracks propagation of different orientations, to be more representative of the fiber reinforcement mechanisms in this type of FRC structure [31].

The insufficient knowledge of steel fiber corrosion contributes to a conservative design philosophy, which limits the mobilization of the full potential of SFRC [32]. Knowledge of RSFRC is even less consolidated. Investigation in this domain is only some few years old and further research is needed. In particular, research on the durability of RSFRC is almost non-existent, particularly with respect to the

corrosion behavior. Therefore, understanding the mechanical and durability performance of RSFRC exposed to chloride attack will help move towards a more rational design and accurate prediction of the long-term performance of the composite under aggressive chloride exposure conditions.

The main purpose of this experimental study is to assess the effects of chloride attack on the post-cracking response of RSFRC by performing double edge wedge splitting tests (DEWSTs) and round panel tests (RPTs). For this purpose, different periods of chloride immersion were adopted for RSFRC specimens prior to testing. The influence of RSF distribution and orientation on the post-cracking behavior of RSFRC after chloride exposure was investigated by image analysis.

The chloride diffusion into uncracked RSFRC was also investigated by means of rapid non-steady chloride migration tests, as well as natural immersion in chloride solution. Additionally, the critical chloride concentration corresponding to the beginning of fiber corrosion, and the prediction of the long-term chloride penetration depth into an uncracked RSFRC structural element subjected to dry-wet cycles in chloride solution were estimated based on the Fick's 2nd law.

2. Experimental Program

2.1. Materials and Mix Compositions

In the current experimental program, two RSFRC mixtures were produced, using ordinary Portland cement type CEM I 42.5R, fly ash (FA), limestone filler (LF), fine river sand (FS) (maximum aggregate size of 1.19 mm and fineness modulus of 1.91), coarse river sand (CS) (maximum aggregate size of 4.76 mm and fineness modulus of 3.84), crushed granite (CG) (maximum aggregate size of 19.10 mm and fineness modulus of 7.01), water (W), two types of polycarboxilate-based superplasticizer with the commercial designations ViscoCrete® 3005 from Sika® (SP1) and MasterGlenium SKY 617 from BASF (SP2), and recycled steel fibers (RSF).

The RSF used in this research were recovered by a shredding process of post-consumed truck tires. These RSF have irregular geometry with various lengths and diameters (Figure 1a,b). The steel was separated from the rubber by an electromagnetic separator, and most of the RSF still contain some rubber particles attached to its surface (Figure 1c). Table 1 presents the average values of the geometric properties of RSF obtained by statistical analysis on a sample of 2000 fibers. The average tensile strength of RSF obtained from direct tensile tests is also presented in Table 1.

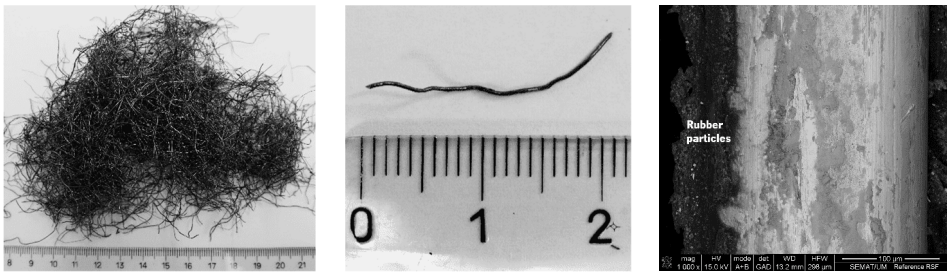

(**a**) (**b**) (**c**)

Figure 1. Recycled steel fibers: (**a**) general view of multi RSF (**b**) general view of the geometry of a single RSF (**c**) SEM micrograph of the surface of a single reference RSF (Magnification: 1000x).

Table 1. Geometric and mechanical properties of RSF.

Properties	RSF
Length, l_f (mm)	20
Diameter, d_f (mm)	0.25
Aspect ratio, l_f/d_f	110
Tensile strength (MPa)	2648

The mix design method for RSFRC was based on the packing density optimization, which follows three main steps [33,34]: i) definition of the proportion of constituent materials for developing an optimized paste; ii) determination of the optimum volume percentage of each type of aggregate in the granular skeleton of the concrete; iii) assessment of an optimum correlation between the binder paste and the solid skeleton in order to obtain RSFRC with the intended properties at fresh and hardened stages, in accordance with the RSFRC structural requirements. Table 2 includes the two compositions of RSFRC, herein designated by "RSFRC0.8%" and "RSFRC1%", produced with a fiber content of 0.8% and 1% in volume of concrete, respectively. The RSFRC0.8% was previously developed by other researchers that used the same materials [23] and was used to cast the specimens produced for the DEWST tests. The RSFRC1% was a new composition developed to produce a more efficient and sustainable concrete, by using a high content of RSF and a partial replacement of paste mass by fly ash. Two different superplasticizers (SP1 and SP2) were used since it was decided to keep the type of superplasticizer (SP1) previously used in RSFRC0.8% production [23], being different from the one used in RSFRC1% (SP2). The RSFRC1% was used to cast the round panels produced for RPTs. In Table 2, w/c is the water/cement ratio.

Table 2. Mix proportions for 1 m^3 of RSFRC.

Concrete Mixture	CEM (kg)	FA (kg)	LF (kg)	W (L)	SP1 (L)	SP2 (L)	FS (kg)	CS (kg)	CG (kg)	RSF (kg)	W/C (-)
RSFRC0.8%	380.5	-	353	140	7.8	-	237	710	590	60	0.37
RSFRC1%	400	200	-	173	-	7.2	148	735	597	76	0.43

2.2. *Test Procedures*

2.2.1. Specimen Preparation and Exposure Conditions

For DEWST tests, six φ150 × 300 mm cylinders were casted with RSFRC0.8% mixture. After 28 days of curing, three cylinders were immersed in a 3.5 wt.% NaCl (0.6 M) solution in order to induce chloride attack, and another three reference cylinders were only cured in water saturated with calcium hydroxide (to prevent any leaching of lime from the specimens during the curing), for comparison purposes. For each pair of cylinders (one submitted to chloride attack and one reference), the following exposure periods were adopted for chloride/water immersion: 10 days; 3 months; 6 months. After the exposure periods, four specimens of φ150 × 60 mm were obtained from each cylinder for the DEWST, as shown in Figure 2. Following the procedure adopted by di Prisco et al. [35], a V-shaped groove with 45° inclination was executed at the extremities of the notched plane, as illustrated in Figure 2 (Notch 1). This V-shaped groove has the objective of inducing a stress field corresponding to an almost pure mode I fracture in the notched plane. In each specimen, 5-mm-deep notches were executed parallel to the loading direction, in order to set the specimen's fracture surface along the notched plane (Notch 2 in Figure 2).

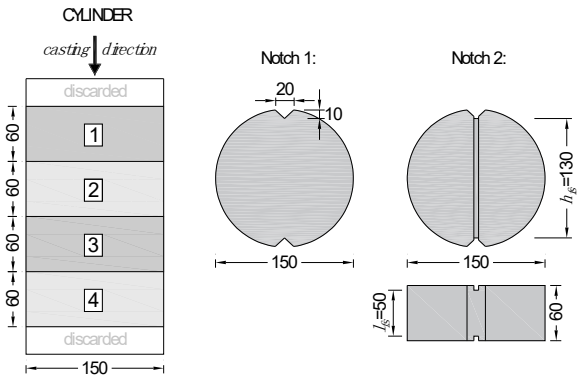

Figure 2. Schematic representation of the preparation process of DEWST specimens. From φ150 × 300 mm cylinders (units in mm).

Twelve round panels with φ600 × 60 mm were casted with the RSFRC1% mixture detailed in Table 2. According to the recommendations of ASTM C1550-08 [36], small RSFRC panels were produced in order to facilitate their handling and placing. According to Minelli and Plizzari [37], such reduction of the panel's diameter and thickness does not affect the scatter and repeatability of the test results.

After 28 days of curing in the lab environment, six panels were immersed in a 3.5 wt.% NaCl solution for chloride attack induction. For comparison purposes, other six reference panels were only cured in water. For each group of three panels, the following exposure conditions were adopted: 10 days of immersion (Cl^- and REF); 3 months of dry-wet cycles in chloride solution (Cl^-)/water immersion (REF).

Additionally, six φ100 × 50 mm cylinders of RSFRC1% were used for the accelerated migration tests described in Section 2.2.5. For comparison purposes, six φ100 × 50 mm cylinders of plain concrete (PC) were also casted with the same cement matrix composition of RSFRC1%.

For the determination of the resistance to chloride penetration by natural immersion, two 150 mm cubic specimens of both RSFRC1% and PC were produced. Two φ100 × 50 mm cylinders of both RSFRC1% and PC were also considered for determining the aging coefficients of RSFRC1%, based on the colorimetric method.

2.2.2. Splitting Tensile Test

The splitting tests were conducted under displacement control, using an external LVDT (Linear Variable Differential Transformer) that was positioned on the actuator to control the vertical deformation of the specimen. The tests were performed with relatively low displacement rates, making it possible to obtain a stable response once the crack process was initiated. The following displacement rates were adopted: 1.0 μm/s up to the displacement of 2.0 mm; 2.0 μm/s from 2.0 mm up to 3.0 mm; 4.0 μm/s until the end of the test.

Each specimen was positioned between two rigid supports and subjected to a diametral compressive line load applied along the thickness of the specimen (Figure 3). For an accurate detection and tracking of the crack propagation, five LVDTs were used to measure the crack opening displacement along the fracture surface (Figure 3a)—three on the front face and two on the rear face of the specimen. The load was registered by means of a 150 kN load cell. The test setup was defined as carried out by Lameiras et al. [38], based on the combination of the DEWST methodology proposed by di Prisco et al. [35] for indirect evaluation of the mode I fracture properties of FRC and the Modified Splitting Tensile Test (MSTT) introduced by a group of researchers from the University of Minho [39,40]. The DEWST was conceived in order to deviate the compressive stresses from the ligament between the tips of the two V-notches mentioned above (Figure 2), while a unique fracture plane is likely to be obtained (Figure 3) [35,38]. After testing, the effective fiber content was evaluated in each of the two fracture surfaces of the split specimen, by counting the number of effective fibers crossing the fractured surfaces. The fiber was considered effective when its length was visible, therefore assuming this fiber has failed by pull-out.

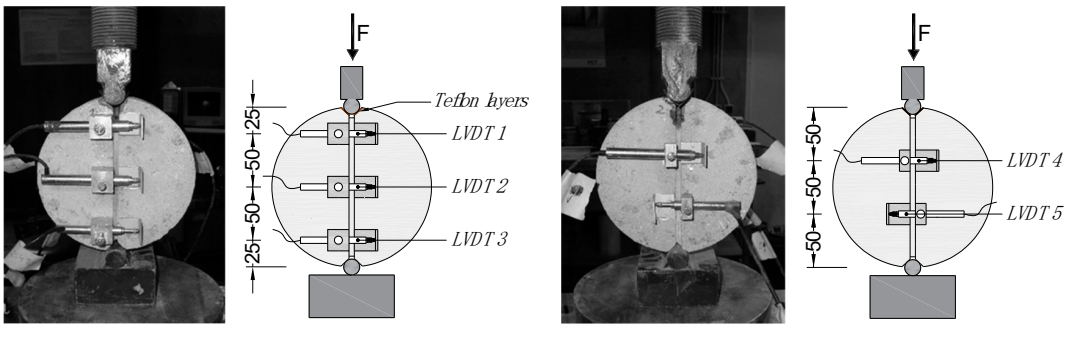

Figure 3. Test setup for DEWST: (**a**) Specimen front view (**b**) Specimen back view (units in mm).

2.2.3. Round Panel Test (RPT)

The RPTs were conducted on round panels supported on three symmetrically arranged pivots, as presented in Figure 4a. The connection between the panel and each pivot was provided by two round steel plates, with a spherical seat machined into the two surfaces to achieve the ball connection recommended by ASTM C1550-08 [36]. Two Teflon sheets were used between the concrete panel and each round steel plate to reduce friction. The load was applied to the panel's center through a hemispherical-ended steel piston at a constant rate of displacement. The central deflection of the panel was measured by an LVDT with a linear stroke of +/− 50 mm installed at the bottom surface of the panel (Figure 4a). Three LVDTs with a linear stroke of +/− 5 mm were also positioned in the bottom surface of the panels to measure the developed crack widths (Figure 4b).

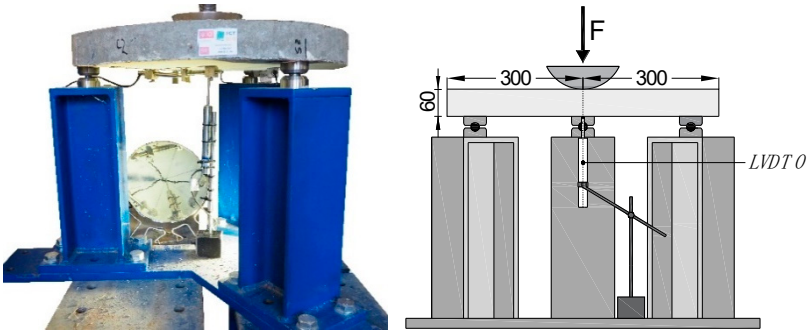

(**a**)

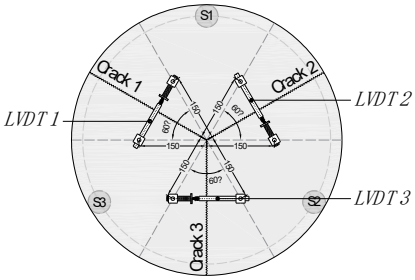

(**b**)

Figure 4. Test setup for RPT: (**a**) Position of the LVDT for central deflection measurement. (**b**) Position of the LVDTs for crack width measurement (units in mm).

2.2.4. Fiber Distribution and Orientation

For a better understanding of the residual stresses and energy absorption obtained in DEWSTs and RPTs, the fiber dispersion and orientation parameters were determined by executing image analysis on plane surfaces of the tested specimens (cut as close as possible to the fracture surface), according to the procedure adopted by Abrishambaf and Cunha [30,41]. This method consists of recognizing the cross section of each RSF, from the surrounding matrix, by image processing of high-resolution pictures taken from the cut surface of the specimens. Taking advantage of the reflective properties of RSF, the best circle/ellipse is fitted to each cross section of RSF. The number of circles/ellipses, the center of gravity and the minor and major diameters of each individual fitted circle/ellipse were computed for determining the orientation and segregation factors. Details about this image analysis procedure can be found elsewhere [28,39].

After computation of the image analysis results, the following parameters that characterize the fiber structure were derived out: i) The number of fibers per unit area, N^f, which corresponded to the ratio between the total number of fibers counted in all analyzed pictures of cut surface (number of all the fitted circles/ellipses) and the total area of the cut surface; ii) Fiber orientation factor, η, which was

calculated with two different approaches. In the first approach, this parameter was determined based on the image analysis procedure of the cut surface, η_{img}, using the following Equation [30]:

$$\eta_{img} = \frac{1}{N_T^f} \sum_{i=1}^{N_T^f} cos\theta_i \quad (1)$$

where θ_i is the angle between the fiber's longitudinal axis and the orthogonal to the cut section, which was computed with the major (a_f) and minor (b_f) axis lengths of the elliptical cross section [42]:

$$\theta_i = \cos^{-1}\left(b_f / a_f\right) \quad (2)$$

In the second method, the average orientation factor within a cross section, $\eta_{\exp}$, was obtained from Equation (3), proposed by Soroushian and Lee [43]:

$$\eta_{\exp} = N^f \frac{A_f}{V_f} \quad (3)$$

where A_f and V_f are the cross sectional area of a single RSF and the volumetric percentage of fibers added to concrete, respectively.

2.2.5. Non-Steady-State Rapid Chloride Migration Test

The accelerated non-steady state migration test method (RCMT), according to the standard NT BUILD 492 [44], was applied to assess the resistance of RSFRC against chloride penetration. The principle of this test is to axially apply an external electrical potential across the specimen by forcing the outside chloride ions to migrate into the specimen (Figure 5a,b). The catholyte solution is 10% NaCl by mass in tap water and the anolyte solution is 0.3 N NaOH in distilled water (Figure 5a). The solutions are stored at 20–25 °C. After the test duration, the specimens are axially split, and a silver nitrate solution (0.1 N $AgNO_3$) is sprayed on to one of the freshly split sections (Figure 5c).

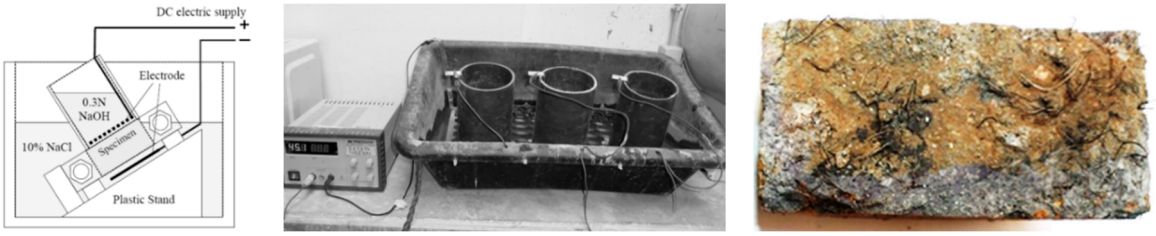

(**a**) (**b**) (**c**)

Figure 5. Rapid chloride migration test: (**a**,**b**) Test setup. (**c**) Split section of RSFRC specimen

The chloride penetration depth is measured from the visible silver chloride precipitation and the chloride migration coefficient, D_m ($\times 10^{-12}$ m^2/s), is calculated from the following simplified equation [44]:

$$D_m = \frac{0.0239\ (273+T)\times L}{(U-2)\times t}\left(x_d - 0.0238\sqrt{\frac{(273+T)\times L \times x_d}{U-2}}\right) \quad (4)$$

where T is the mean value between initial and final temperature (°C) of the anolyte solution during the test, U is the absolute value of the applied voltage (V), L is the thickness of specimen (mm), t is the test duration (hours) and x_d is the average chloride penetration depth (mm).

2.2.6. Immersion Test in NaCl Solution

The determination of the resistance to chloride penetration by natural immersion was performed according to the standards ASTM C1556-03 [45] and NT BUILD 443 [46]. The method is based on determining parameters related to chloride penetration in hardened concrete, from chloride penetration profiles obtained after immersion in 3.5 wt.% NaCl solution. The faces of each cubic specimen and cylinder were waterproofed with a single layer coating of a polyurethane-based resin, except for one that allows the penetration of chlorides (Figure 6a).

(**a**) (**b**) (**c**)

Figure 6. Chloride penetration test by immersion: (**a**) Immersion of the specimens in chloride solution. (**b**) Collection of powder samples of concrete at different depths in the specimens. (**c**) Using the Kit RCT-500 to determine the chloride content.

After 90 days of immersion (Figure 6a), the determination of the chloride concentration at different depths in the cubic specimens was performed using the kit RCT-500 (Rapid Chloride Test) of the German Instruments A/S. The RCT-500 consists of a quick and easy-to-use kit for determination of chloride content as a percentage of binder mass (cement + fly ash). In this case, the acid soluble amount of chlorides (total chlorides = free chlorides + physical bound chlorides) was measured on 1.5 g powder concrete samples collected at various depths by drilling the test specimens with a 22 mm drill bit (Figure 6b). Each powder sample was attacked to extract the chloride ions, and the chloride content was obtained by using the RCT electrode calibrated with four calibration solutions of known chloride content (Figure 6c). In each test specimen, one chloride profile was determined from 10–14 powder samples collected at different depths.

After obtaining the chloride content profile for each concrete specimen, the values of the surface chloride content, C_s (% of binder mass), and the apparent chloride diffusion coefficient, D_d ($\times 10^{-12}$ m^2/s), were determined by curve-fitting the measured chloride-ion contents to an error-function solution of Fick's 2nd law, according to the following Equation [46]:

$$C_x = C_s - (C_s - C_0) erf\left(\frac{1/2\, x}{\sqrt{D_d \times t}}\right) \quad (5)$$

where C_x is the chloride content (% of binder mass) measured at depth x (m) for a exposure time of immersion t (s), C_s is the chloride content (% of binder mass) calculated by regression analysis at the concrete surface after a time of immersion t (s), C_0 is the initial chloride content in concrete prior to submersion in the exposure solution (it was assumed 0% as set by Frederiksen et al. [47]) and erf is the error-function.

The variation of the chloride diffusion coefficient with time supposes a decrease attributed to the refinement of the pore structure of concrete, which can be very significant and is expressed by the age coefficient. For the determination of the aging coefficients of the RSFRC1% and PC, considering the chloride diffusion coefficients calculated by the colorimetric method, one φ100 × 50 mm cylinder of RSFRC and other of PC were submitted to 10 days of continuous immersion and the remaining two specimens (one of RSFRC and one of PC) were subjected to 3 months of continuous immersion. After these exposure periods, the specimens were axially split, and a silver nitrate ($AgNO_3$) solution was sprayed on to one of the freshly split sections.

The chloride penetration depth was measured from the visible white silver chloride precipitation, where free chlorides have penetrated into concrete. The values of the chloride diffusion coefficient, D_c, were determined according to the assumptions indicated by Yang et al. [48], considering the following equation:

$$D_c = \frac{-x_c^2}{2\ln\left(\frac{C_c}{C_0}\right)t} \quad (6)$$

where x_c is the colorimetric penetration depth (m), C_c is the concentration of free chlorides in the pore solution corresponding to the colour change boundary (N), C_0 is the chloride concentration ponded at the top surface (N) and t is the exposure time in seconds.

The specimens were subjected to continuous ponding with 3.5 wt.% NaCl solution, which corresponds to a chloride concentration of C_0= 0.61 N (considering that C_0= 0.52 N for 3.0 wt.% NaCl solution [48]). The free chloride concentration at the color change boundary was set equal to C_c= 0.07 N, as pointed out in [44,49,50] for Ordinary Portland Cement (OPC) concrete.

The aging coefficient, n_{cl}, was determined considering the following Equation [51,52]:

$$n_{cl} = \frac{\ln\left(\frac{D_{c,1}}{D_{c,2}}\right)}{\ln\left(\frac{t_2}{t_1}\right)} \quad (7)$$

where $D_{c,1}$ and $D_{c,2}$ are the chloride diffusion coefficients corresponding to 10 days (t_1) and 3 months (t_2) of chloride immersion, respectively.

Additionally, for comparison purposes, the chloride diffusion coefficients were also calculated by the colorimetric method in the cubic specimens used for the determination of chloride profiles (Figure 6). The chloride concentration corresponding to the chloride penetration depth in RSFRC and PC cubes was determined by the Fick's 2nd law (Equation (5)), considering the parameters C_s and D_d obtained from the chloride profiles.

3. Results and Discussions

3.1. Long-Term Effects of Chloride Attack on the Post-Cracking Behavior of RSFRC

3.1.1. Splitting Tensile Tests

After the exposure periods of DEWST specimens to chloride immersion, the formation of corroded material in the 3.5 wt.% NaCl solution was observed, as well as corrosion spots at the exposed surfaces of cylinders. After DEWSTs, the chloride penetration depth was evaluated by spraying an broken surface orthogonally to the fracture surface with silver nitrate solution. Average internal depths of chloride penetration of 6.1, 19.5 mm and 28.1 mm were measured after 10 days, 3 months and 6 months of chloride immersion, respectively. No significant signs of corrosion in the RSF at the fracture surface were detected. Only some few fibers near the exposed surface seemed to corrode.

Figure 7a shows the average splitting tensile stress versus crack mouth opening displacement (CMOD) curves, $\sigma_{t,split} - \omega$, obtained in DEWSTs after submitted the specimens to chloride immersion (Cl^-) and to curing in water (REF). Figure 7b depicts the relationship between the crack width, ω, and the corresponding energy absorption during the fracture process, $G_{F\omega}$, which corresponds to the area under the $\sigma_{t,split} - \omega$ curve. According to Figure 7a,b, the chloride attack led to the increase of $G_{F\omega}$ in specimens submitted to 10 days of chloride immersion. However, after 6 months of chloride immersion, the opposite occurred for all the crack opening levels at which the energy absorption was evaluated. After 3 months of chloride immersion, the chloride attack had no significant influence on the $G_{F\omega}$, when compared to reference specimens. The $G_{F\omega}$ values were similar for all reference RSFRC specimens.

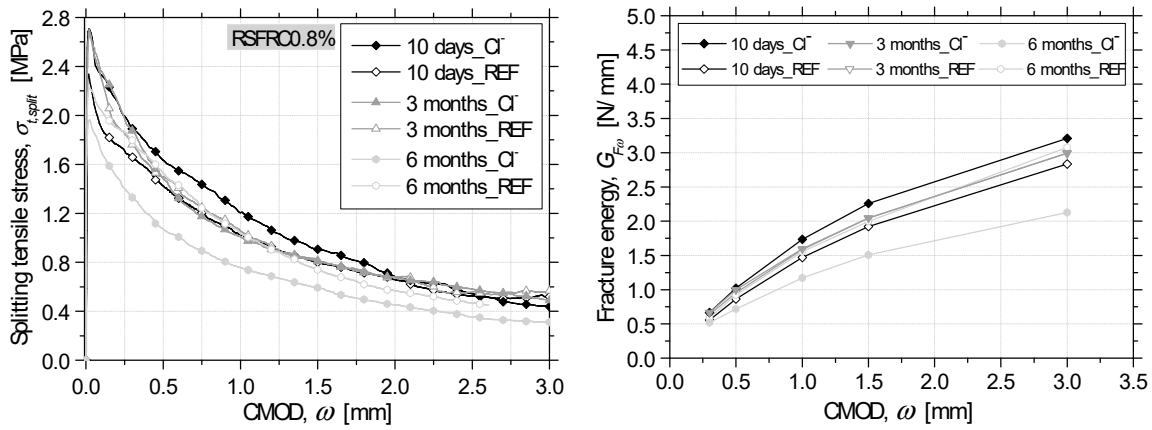

Figure 7. Results of DEWST tests: (**a**) Average $\sigma_{t,split} - \omega$ curves (**b**) $G_{F\omega} - \omega$ relationship.

3.1.2. Fiber Distribution/Orientation Profiles

Table 3 includes the fiber distribution and orientation parameters obtained on the failure surface of two specimens (one Cl^- and one REF) for each different exposure period. For a better analysis of the values of N^f, the corresponding $\sigma_{t,split} - \omega$ curves registered in the indicated specimens (Table 3) are depicted in Figure 8.

Table 3. Fiber distribution and orientation parameters for the analyzed specimens after DEWST.

Test Series	Specimen (Figure 2)	N^f (fibers/cm^2)	η_{img}	η_{exp}
10 days_Cl^-	3	9.36 (74% [1])	0.623	0.574
10 days_REF	2	6.42 (76% [1])	0.619	0.394
3 months_Cl^-	4	5.95 (74% [1])	0.560	0.365
3 months_REF	4	8.08 (82% [1])	0.562	0.496
6 months_Cl^-	2	6.17 (68% [1])	0.613	0.378
6 months_REF	2	7.04 (69% [1])	0.602	0.4326
Average		7.17 (74% [1])	0.596	0.440
CoV (%)		18.39	4.76	18.40

[1] Percentage of fibers failed by tensile rupture.

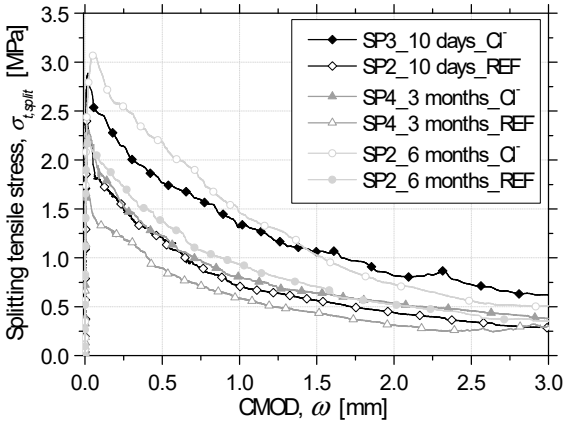

Figure 8. $\sigma_{t,split} - \omega$ curves registered in the corresponding specimens (SP) of the fiber distribution/orientation analysis (Table 3).

According to Table 3 and Figure 8, the higher value of N^f obtained in SP3_10 days_Cl^- compared to SP2_10 days_REF corroborates the corresponding $\sigma_{t,split} - \omega$ curves, which means that the differences

between the $\sigma_{t,split}$ obtained in the specimens submitted to 10 days of immersion (Cl^-&REF) are essentially explained by the effective fiber content in the failure surface. For the exposure period of 3 months, the SP4 submitted to chloride attack showed a lower number of RSF in the cut surface than the reference SP4. However, higher values of $\sigma_{t,split}$ were observed in the SP4_3 months_Cl^- compared to SP4_3 months_REF (Figure 8), which may be due to a beneficial effect of chloride attack in terms of the fiber pull-out performance. The SP2 submitted to the exposure period of 6 months showed similar N^f. However, a smaller $\sigma_{t,split}$ is observed in SP2_6 months_Cl^- (Figure 8), which may be attributed to a detrimental effect of chloride attack on the fiber pull-out performance.

Table 3 presents an estimation of the percentage of fibers failed by tensile rupture, which on average was significant due to the irregular geometry of RSF and the strong RSF-matrix bond.

In terms of the fiber orientation factor obtained by image analysis, η_{img}, similar values were obtained for test series of 10 days and 6 months. A slight decrease of η_{img} was observed in test series of 3 months, which means that the fibers were less orthogonally aligned to the cut plane. This fact is in agreement with the lower peak values of $\sigma_{t,split}$ obtained in the reference specimens. The orientation factor computed from the image analysis approach, η_{img}, is higher than the correspondent $\eta_{\exp}$.

3.1.3. Round Panel Tests

After 10 days of chloride immersion, no significant signs of superficial corrosion were visible in the RSFRC panels, and only some uncovered fibers located on the exposed surfaces appeared to be corroded. However, after 3 months of dry-wet cycles in chloride solution, a significant increase in surface corrosion has occurred on the RSFRC panels and many corrosion spots were visible due to the uncovered RSF located at exposed surfaces that were directly in contact with the chloride solution.

After RPTs, the crack surfaces were sprayed with silver nitrate solution to assess the chloride penetration depth. Average internal chloride penetration depths of 7.0 and 9.5 mm were measured after 10 days of chloride immersion and 3 months of dry-wet cycles in chloride solution, respectively. Few corrosion spots were detected by microscopic inspection on RSF near the exposed surfaces, located on an orthogonal cut surface to a crack surface, as observed in Figure 9a,b.

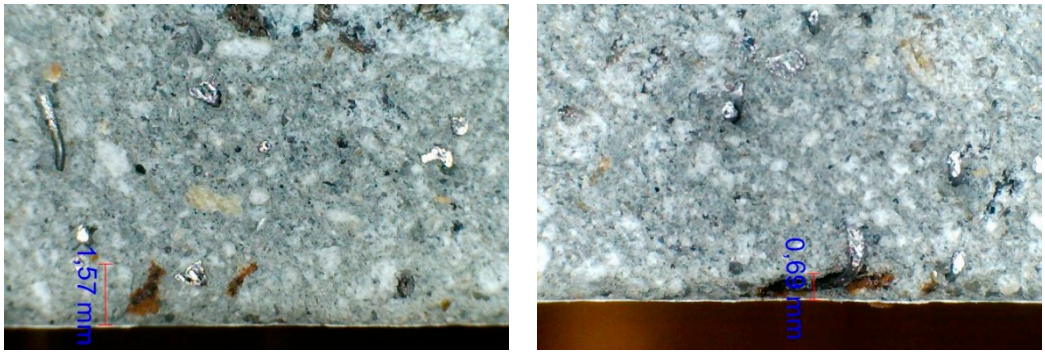

(**a**) (**b**)

Figure 9. Corrosion signs on RSF near the exposed surfaces of panels after the exposure period of: (**a**) 10 days (**b**) 3 months.

Figure 10a shows the average force-central deflection responses, $F-\delta$, registered in RPTs of RSFRC1% panels, after the environmental exposure periods of 10 days of immersion (Im_Cl^- and Im_REF) and 3 months of dry-wet cycles in chloride solution (DW_Cl^-)/water immersion (Im_REF). The average values of energy absorbed, W, at central deflections, δ, of 5, 10 and 20 mm are represented in Figure 10b. These W values were corrected considering the panel thickness by using the following equation recommended by ASTM C1550-08 [36]:

$$W = W'\left(\frac{t_0}{t}\right)^{\beta}\left(\frac{d_0}{d}\right) \text{ with } \beta = 2.0-(\delta-0.5)/80 \quad (8)$$

where W is the corrected energy absorption (J), W' is the measured energy absorption (J), t_0 is the nominal thickness of 75 mm, t is the panel thickness (mm), d_0 is the nominal diameter of 800 mm, d is the panel diameter (mm) and δ is the specified central deflection at which the capacity to absorb energy is measured (mm).

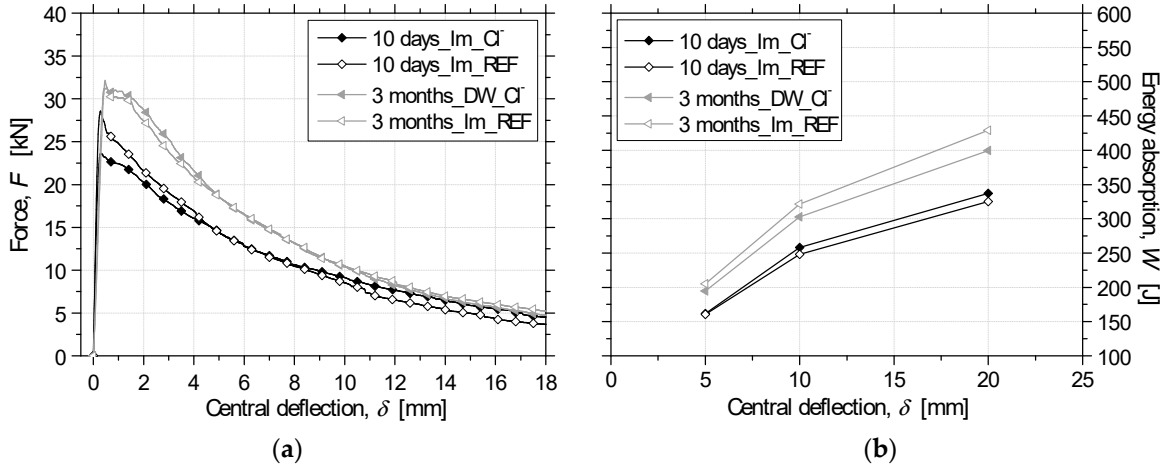

Figure 10. Results of RPTs: (**a**) Average $F - \delta$ curves (**b**) $W - \delta$ relationship.

According to Figure 10a, the panels submitted to 10 days of chloride immersion showed lower average post-cracking resistance than reference panels and after 3 months of aggressive chloride exposure conditions, the post-cracking resistance of the RSFRC panels was similar to that of the reference panels. However, as no significant signs of RSF corrosion were visible at the crack surfaces of the panels, the differences between the $F - \delta$ curves of Cl^- and REF panels may be explained by the slight differences in panel thickness and/or due to fiber distribution and orientation.

A slightly higher energy absorption was obtained for panels submitted to 10 days of chloride immersion regarding their reference panels, while a lower energy absorbed was shown by the panels submitted to 3 months of environmental exposure, compared to reference panels. This could be indicative of corrosion effects of RSF. However, as no significant signs of RSF corrosion were detected at crack surfaces, it seems that these differences in energy absorption (Cl^- and REF specimens) for each exposure period are mainly related to the fiber distribution at crack surfaces.

3.1.4. Fiber Distribution/Orientation Profiles

Table 4 includes the fiber distribution and orientation parameters obtained on one cut surface of each two round panels (one Cl^- and one REF) at each different exposure period. For a better analysis of the values of N^f, the corresponding energy absorption registered in the analyzed panels is depicted in Table 5.

Table 4. Fiber distribution and orientation parameters for the analyzed panels after RPT.

Test Series	Crack (Figure 4b)	Panel Thickness (mm)	N^f (Fibers/cm^2)	η_{img}	η_{exp}
10 days_Im_Cl^-	1	63.41	10.82 (76% [1])	0.625	0.531
10 days_Im_REF	1	67.65	7.69 (74% [1])	0.629	0.377
3 months_DW_Cl^-	2	64.64	9.33 (77% [1])	0.619	0.458
3 months_Im_REF	2	66.42	8.73 (81% [1])	0.628	0.429
Average		65.53	9.14 (77% [1])	0.625	0.449
CoV (%)		2.86	14.30	0.72	14.32

[1] Percentage of fibers failed by tensile rupture.

Table 5. Energy absorption obtained in the corresponding panels of the fiber distribution/orientation analysis (Table 4).

Test Series	W_5 (J)	W_{10} (J)	W_{20} (J)	W_{40} (J)
10 days_Im_Cl^-	150.94	248.89	353.18	424.40
10 days_Im_REF	139.12	216.53	271.36	-
3 months_DW_Cl^-	178.78	286.80	379.42	432.00
3 months_Im_REF	218.13	344.21	452.90	515.34

According to the results presented in Tables 4 and 5, for 10 days of immersion, it seems that the chloride attack had a negligible effect, because the higher values of W obtained for the panel 10 days_Im_Cl^-, compared to the corresponding reference panel (10 days_Im_REF), are justified by the higher N^f measured at the cut surface. After 3 months of environmental exposure, a similar value of N^f was obtained for chloride-attacked and reference panels. However, higher energy absorption was obtained in the reference panel (3 months_Im_REF).

As the fiber distribution was determined for only one cut surface (one crack) of each analyzed panel, the differences between the energy absorption presented in Table 5 may also be justified by the proportion of the fibers on the other two crack surfaces of the panels. In this sense, the average crack width vs. energy absorption relationships, $\omega - W$, obtained in each analyzed panel are represented in Figure 11. As observed, the $\omega - W$ relationships are in agreement with the results of energy absorption presented in Table 5, which means that the chloride attack had a negligible effect for these two exposure periods. The differences between the values of energy absorption appeared to be justified by the effective fiber content at fracture surfaces.

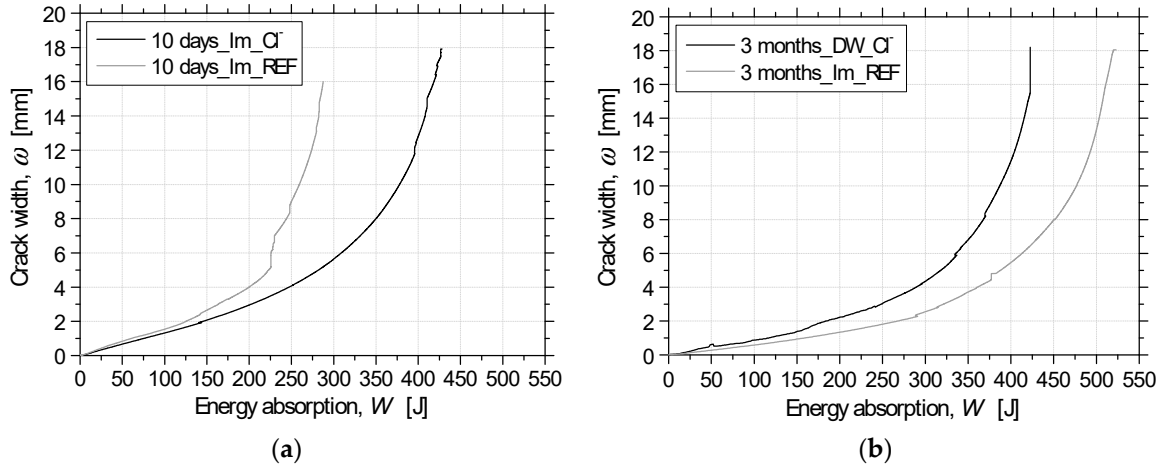

Figure 11. Average $\omega - W$ relationship for analyzed panels from RPTs after the exposure period of: (**a**) 10 days; (**b**) 3 months.

In Table 4, the average percentage of fibers failed by rupture was similar to that obtained in the analyzed DEWST specimens (Table 3). The obtained values of η_{img} and $\eta_{\exp}$ did not significantly vary between panels, which means that no significant differences in fiber orientation occurred. The obtained values of η_{img} were higher than the correspondent $\eta_{\exp}$, as also found in DEWST specimens, which may be justified by the higher difficulty of detecting the N^f according to this approach.

3.2. Durability Indicators of RSFRC under Chloride Exposure

Non-Steady-State Rapid Chloride Migration

The average RCMT chloride diffusion coefficient, D_m, obtained in RSFRC1% and in the corresponding plain concrete (PC) (before RSF addition) is shown in Table 6, indicating that the

RSF slightly decreased the resistance to chloride penetration. One hypothesis may be the increase of the open porosity of concrete with the addition of steel fibers [8], which provides higher chloride penetration, mainly through the fiber-matrix interfaces of the fibers located at the exposed surface of the specimens. In addition, the method for evaluating the chloride diffusion by migration, despite being faster than the one based on diffusion by natural immersion, may be not adequate for RSFRC. The potential difference applied, and the duration of test are defined according to some preliminary measures of current intensity obtained in plain concrete, but the presence of steel fibers can significantly influence the electrical field generated due to the high electrical conductivity of steel fibers. Thus, it is more prudent to use diffusion methods, based on the natural immersion, to evaluate the penetration of chlorides in RSFRC, which better simulates the usual environmental exposure conditions.

Table 6. Chloride migration coefficients in RSFRC1% and PC specimens.

	RSFRC1%	PC
D_m ($\times 10^{-12}$ m^2/s)	14.94	11.74
CoV (%)	13.60	22.74

3.3. Resistance to Chloride Penetration by Immersion

3.3.1. Chloride Profiles

The chloride profiles obtained in each cubic specimen of RSFRC1% and PC are presented in Figure 12, determined as described in Section 2.2.6.

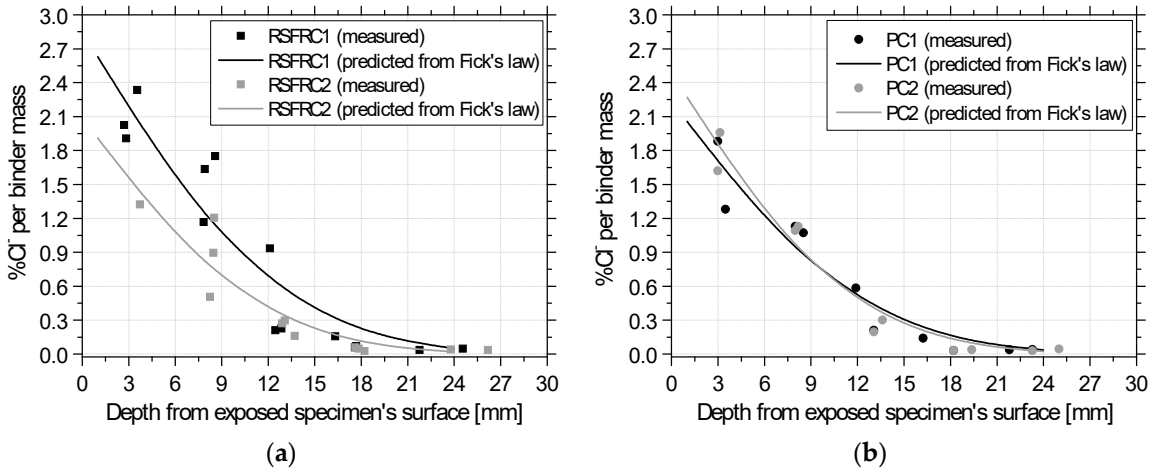

Figure 12. Chloride profiles along specimen depth from exposed surface of specimens (**a**) RSFRC1% and (**b**) PC.

The obtained average surface chloride content, C_s, and the apparent chloride diffusion coefficient, D_d, determined by curve-fitting the measured chloride-ion contents to Fick's 2nd law (Figure 12), are presented in Table 7.

Table 7. Chloride diffusion by immersion determined by Fick's 2nd law.

Concrete	C_s (%)	D_d ($\times 10^{-12}$ m^2/s)
RSFRC1%	2.472	6.02
PC	2.361	5.92

The obtained values of C_s and D_d evidence a similar resistance to chloride penetration between RSFRC and PC specimens, which means that the presence of RSF had a negligible effect in the

penetration of chloride ions into concrete. Lower values were obtained for D_d compared to D_m (Table 6). The same trend is reported in the literature for PC [53,54]. For RSFRC, the higher values of D_m are also due to the mentioned influence of steel fibers in the chloride migration test method.

3.3.2. Chloride Diffusion and Aging Coefficient by Colorimetric Method

Table 8 presents the results obtained for chloride diffusion and aging coefficients evaluated by colorimetric method in RSFRC and PC cylindrical and cubic specimens previously submitted to chloride immersion, as described in Section 2.2.6.

Table 8. Chloride diffusion by immersion determined by colorimetric method.

Test series	Cylindrical Specimens		Cubic Specimens
	D_c ($\times 10^{-12}$ m^2/s)	n_{cl}	D_c ($\times 10^{-12}$ m^2/s)
RSFRC_10 days	8.31	0.56	-
RSFRC_3 months	2.42		3.26
PC_10 days	7.34	0.49	-
PC_3 months	2.48		2.49

As expected, the chloride diffusion coefficient, D_c, decreased with the time of exposure for both RSFRC and PC cylindrical specimens. No significant differences were observed between the aging coefficients of RSFRC and PC.

After 3 months of chloride immersion, the values of D_c obtained by the colorimetric method in cubic specimens were lower than those of D_d obtained by the Fick's 2nd law (Table 7). This may be explained by the unrealistic surface chloride content, C_0, assumed for the determination of D_c. The C_0 was assumed equal to the chloride concentration of NaCl solution, instead of being considered the chloride concentration in the surface pore solution, which is a lower value due to the chloride binding.

The average chloride content (total amount) obtained by Fick's 2nd law at the chloride penetration depth in RSFRC (10.5 mm) and PC cubes (9.1 mm) was 0.7% and 0.8% per binder mass for RSFRC and PC, respectively.

According to Otsuki et al. [55], a total amount of chlorides of 0.4–0.5% by cement mass was found at the color change boundary in OPC concrete after immersing in NaCl solution. According to these authors [55], it seems that the obtained results in RSFRC agree with the concentration of chlorides reported in OPC concrete.

3.3.3. Critical Chloride Concentration for Fiber Corrosion Initiation in the RSFRC Round Panels

The critical content of chlorides corresponding to the beginning of fiber corrosion was simply estimated in the RSFRC1% round panels that were previously subjected to 3 months of dry-wet cycles in 3.5 wt.% NaCl solution, and then subjected to RPTs. The following procedure was considered:

(1) Knowing the average colorimetric chloride penetration depth measured in the panels (9.5 mm, as mentioned in Section 3.1.2), the chloride diffusion coefficient, D_c, was determined according to Equation (6) with $C_0 = 0.61$ N and $C_0 = 0.52$ N; from those, a value of 2.69×10^{-12} m^2/s was obtained.

(2) Assuming a linear correlation between D_d and D_c, as reported by some authors [48,56], the value of D_d was derived by linear regression, considering the average values of D_d (Table 7) and D_c (Table 8) obtained in RSFRC and PC cubic specimens after 3 months of chloride immersion. The calculated D_d was 5.95×10^{-12} m^2/s.

(3) The surface chloride content, C_s, was determined by the Fick's 2nd law (Equation (5)), considering the value of 0.7% of binder mass for C_x in RSFRC cubic specimens (Section 3.3.2). The value estimated for C_s was 2.157% of binder mass.

(4) The critical chloride content corresponding to the beginning of fiber corrosion, C_{cr}, was determined by the Fick's 2nd law, considering the parameters D_d and C_s obtained in steps 2) and 3), respectively. The average depth of corroded fibers was measured with a USB microscope in a cut surface of the panels after performing RPTs. The value obtained for C_{cr} was 2.05% of binder mass, corresponding to an average depth of corroded fibers of 0.62 mm. A typical critical chloride content in the range of 0.4–1.0 wt.% of cement is reported in the literature for conventional reinforced concrete [10], although it has been found that this may vary as much as 0.17–2.5 wt.% of cement [57]. However, the critical chloride content has been found to be much higher in SFRC [58,59], which is in line with the critical chloride content estimated from this study.

3.3.4. Chloride Penetration Prediction of RSFRC under Chloride Attack

The long-term chloride penetration depth of the critical chloride content estimated in 3.3.2.3. was predicted based on the the Fick's 2nd law (Equation (5)). This prediction was determined considering 2.157% of binder mass for C_s and 2.05% of binder mass for C_{cr} (Section 3.3.3.). The chloride diffusion coefficient, D_d, was defined by using the average aging coefficient of 0.56 obtained for RSFRC specimens (Table 8). The following equation was used to determine D_d for the time dependency [60]:

$$D(t) = D_{ref}\left(\frac{t_{ref}}{t}\right)^m \quad (9)$$

where $D(t)$ is the diffusion coefficient in m^2/s at the exposure time t(s), D_{ref} is the diffusion coefficient at reference time, t_{ref} ($D_{ref} = 5.95 \times 10^{-12}$ m^2/s, t_{ref} = 7,776,000 s), and m is the aging coefficient (0.56—Table 8). Figure 13 shows the long-term prediction of the average penetration depth along time of the critical chloride content of 2.05 wt.% of binder, for the RSFRC studied in this work exposed to dry-wet cycles in 3.5 wt.% NaCl solution. As shown, even after 50 years, the average penetration depth of the critical chloride content is lower than 3 mm, confirming that corrosion of steel fibers is essentially a surface phenomenon.

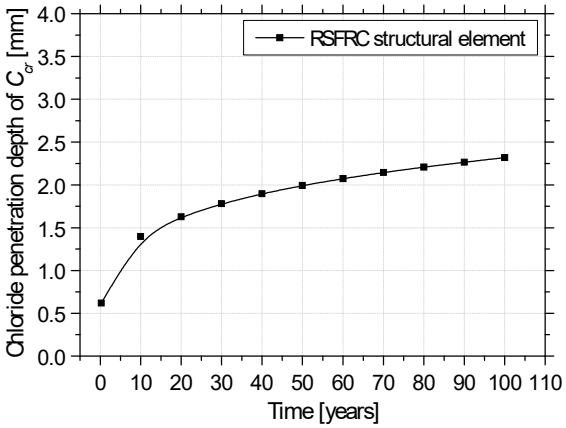

Figure 13. Prediction of the average penetration depth along time of the critical chloride content of 2.05 wt.% of binder, for RSFRC exposed to dry-wet cycles in 3.5 wt.% NaCl solution.

4. Conclusions

DEWSTs and RPTs were carried out to assess the effects of chloride attack on the post-cracking behavior of RSFRC, considering the influence of different chloride exposure periods and fiber distribution/orientation profile. The chloride diffusion in RSFRC was investigated by migration under non-steady-state and natural immersion. A simplified prediction of the critical chloride content corresponding to the beginning of fiber corrosion and the long-term chloride penetration depth into a

RSFRC structural element exposed to a maritime environment (dry-wet cycles in chloride solution) was performed. The main conclusions based on the experimental results are:

(1) For the exposure periods adopted of chloride immersion in 3.5 wt.% NaCl solution, no significant signs of corrosion were detected in the RSF on the fracture surfaces of RSFRC specimens. However, corrosion spots were observed at exposed surfaces of all specimens.

(2) The $\sigma_{t,split} - \omega$ curves obtained for the RSFRC0.8% specimens and the corresponding fiber distribution analysis at crack surfaces revealed for the influence of chloride attack on the post-cracking behavior of RSFRC a negligible effect after 10 days of immersion, a beneficial effect after 3 months of immersion, and a detrimental effect after 6 months of immersion.

(3) The $F - \delta$ responses registered in the RSFRC1% panels and its corresponding fiber distribution analysis at crack surfaces revealed a negligible effect of the chloride attack on the post-cracking behavior of RSFRC after 10 days of immersion and 3 months of dry-wet cycles in chloride solution.

(4) A significant number of fibers ruptured during the execution of tests; no significant differences were detected in terms of the fiber orientation factor between DEWST specimens and round panel tests.

(5) The chloride migration test under non-steady state may not be feasible for RSFRC, since the presence of steel fibers seems to have a significant influence in the test methodology, mainly by inducing severe corrosion in RSF. The determination of the chloride diffusion for RSFRC is more prudent by natural immersion test in salt solution.

(6) The presence of RSF had a negligible effect on the penetration of chloride ions into concrete. The chloride content obtained for the chloride penetration depth was 0.70% and 0.80% per binder mass for, respectively, RSFRC1% and PC cubes previously subjected to 3 months of chloride immersion. The critical content of chlorides corresponding to the beginning of fiber corrosion, obtained in RSFRC1% panels subjected to 3 months of dry-wet in chloride solution, was 2.05% by binder mass. According to the literature, these results are in agreement with the measured concentration of chlorides reported at the color change boundary in OPC concrete and with the critical chloride content reported by some authors for steel fiber reinforced concrete.

(7) A chloride penetration depth of about 2.3 mm was predicted into a RSFRC structural element after exposed to dry-wet cycles in a 3.5 wt.% NaCl solution for 100 years.

Author Contributions: Conceptualization, C.M.V.F.; methodology, C.M.V.F., J.A.B.B. and J.A.B.; formal analysis, C.M.V.F., J.A.B.B. and J.A.B.; resources, C.M.V.F. and J.A.B.B.; data curation, C.M.V.F.; writing—original draft preparation, C.M.V.F.; writing—review and editing, J.A.B.B. and J.A.B.; supervision, J.A.B.B. and J.A.B.; funding acquisition, C.M.V.F. and J.A.B.B.

Funding: This research was funded by C.F. research grant PD/BD/113638/2015 provided by Fundação para a Ciência e a Tecnologia (FCT) through the Doctoral Program in Eco Construction and Rehabilitation—EcoCoRe, and J.B. through the project ICoSyTec (POCI-01-0145-FEDER-027990) financed by FCT.

Acknowledgments: The authors would like to express their sincere gratitude and appreciation to Twincon Company for supplying the recycled steel fibers. The authors wish also to acknowledge the materials supplied by SECIL (cement), SIKA and BASF (superplasticizers), Omya Comital (limestone filler), and PEGOP (Fly ash). Finally, the support provided by CiviTest Company in the production of concrete specimens is also acknowledged. The first two authors acknowledge the financial support provided through the project ICoSyTec (POCI-01-0145-FEDER-027990) financed by Fundação para a Ciência e Tecnologia (FCT) and co-funded by FEDER through Operational Competitiveness and Internationalization Programme (POCI).

Conflicts of Interest: The authors declare no conflict of interest.

References

1. Mehta, P.K.; Monteiro, P.J.M. *Concrete: Microestructure, Properties and Materials*, 3rd ed.; McGraw-Hill: New York, NY, USA, 2006.
2. Bogas, J.; Gomes, A. Non-steady-state accelerated chloride penetration resistance of structural lightweight aggregate concrete. *Cement Concrete Compos.* **2015**, *60*, 111–122. [CrossRef]

3. Bertolini, L.; Elsener, B.; Pedeferri, P.; Polder, R.P. *Corrosion of Steel in Concrete—Prevention, Diagnosis, Repair*, 1st ed.; Wiley-VCH: Weinheim, Germany, 2004; pp. 21–36.
4. Singh, A.P.; Singhal, D. Permeability of steel fibre reinforced concrete influence of fibre parameters. *Procedia Eng.* **2011**, *14*, 2823–2829. [CrossRef]
5. Marcos-Meson, V.; Michel, A.; Solgaard, A.; Fischer, G.; Edvardsen, C.; Skovhus, T.L. Corrosion resistance of steel fibre reinforced concrete—A literature review. *Cement Concrete Res.* **2018**, *103*, 1–20. [CrossRef]
6. Teruzzi, T.; Cadoni, E.; Frigeri, G.; Cangiano, S.; Plizzari, G. Durability aspects of steel fibre reinforced concrete. In Proceedings of the BEFIB'2004—6th International RILEM Symposium on Fibre-Reinforced Concretes (FRC), Varenna, Italy, 20–22 September 2004; pp. 625–634.
7. Roque, R.; Kim, N.; Kim, B.; Lopp, G. *Durability of Fiber-Reinforced Concrete in Florida Environments*; Final Report September 2004–June 2009, UF Project No. 00050493; Dept. of Civil and Coastal Engineering, University of Florida: Gainesville, FL, USA, 2009; 25p.
8. Frazão, C.; Camões, A.; Barros, J.; Gonçalves, D. Durability of steel fiber reinforced self-compacting concrete. *Constr. Build. Mater.* **2015**, *80*, 155–166. [CrossRef]
9. Chen, G.; Hadi, M.N.S.; Gao, D.; Zhao, L. Experimental study on the properties of corroded steel fibres. *Constr. Build. Mater.* **2015**, *79*, 165–172. [CrossRef]
10. Angst, U.; Elsener, B.; Larsen, C.K.; Vennesland, Ø. Critical chloride content in reinforced concrete—A review. *Cement Concrete Res.* **2009**, *39*, 1122–1138. [CrossRef]
11. Berrocal, C.G.; Lundgren, K.; Löfgren, I. Corrosion of steel bars embedded in fibre reinforced concrete under chloride attack: State of the art. *Cement Concrete Res.* **2016**, *80*, 69–85. [CrossRef]
12. Hwang, J.P.; Jung, M.S.; Kim, M.; Ann, K.Y. Corrosion risk of steel fibre in concrete. *Constr. Build. Mater.* **2015**, *101*, 239–245. [CrossRef]
13. Wang, Q.; Sun, W.; Guo, L.; Gu, C.; Zong, J. Modeling chloride diffusion coefficient of steel fiber reinforced concrete under bending load. *Adv. Civ. Eng.* **2018**, *2018*, 3789214. [CrossRef]
14. Balouch, S.U.; Forth, J.P.; Granju, J.-L. Surface corrosion of steel fibre reinforced concrete. *Cement Concrete Res.* **2010**, *40*, 410–414. [CrossRef]
15. Pillai, R.G.; Annapareddy, A. Service life prediction models for chloride-laden concrete structures: A review and nomographs. *Int. J. 3R's* **2013**, *4*, 563–580.
16. Safehian, M.; Ramezanianpour, A.A. Prediction of RC structure service life from field long term chloride diffusion. *Comput. Concrete* **2015**, *15*, 589–606. [CrossRef]
17. Maage, M.; Helland, S.; Poulsen, E.; Vennesland, Ø.; Carlsen, J.E. Service life prediction of existing concrete structures exposed to marine environment. *ACI Mater. J.* **1996**, *93*, 602–608.
18. Khan, M.U.; Ahmad, S.; Al-Gahtani, H.J. Chloride-induced corrosion of steel in concrete: An overview on chloride diffusion and prediction of corrosion initiation time. *Int. J. Corros.* **2017**, *2017*, 5819202. [CrossRef]
19. Pilakoutas, K.; Neocleous, K.; Tlemat, H. Reuse of tyre steel fibres as concrete reinforcement. *Proc. ICE Eng. Sustain.* **2004**, *157*, 131–138. [CrossRef]
20. Aiello, M.A.; Leuzzi, F.; Centonze, G.; Maffezzoli, A. Use of steel fibers recovered from waste tyres as reinforcement in concrete: Pull-out behaviour, compressive and flexural strength. *Waste Manag.* **2009**, *29*, 1960–1970. [CrossRef]
21. Graeff, A.; Pilakoutas, K.; Lynsdale, C.; Neocleous, K.; Peres, M. Fatigue resistance and cracking mechanism of concrete pavements reinforced with recycled steel fibres recovered from post-consumer tyres. *Eng. Struct.* **2012**, *45*, 385–395. [CrossRef]
22. Micelli, F.; Leone, M.; Centonze, G.; Aiello, M. Go green: Using waste and recycling materials. In *Infrastructure Corrosion and Durability—A Sustainability Study*; Lu, Y., Ed.; OMICS Group eBooks: Foster City, CA, USA, 2014; pp. 1–68.
23. Zamanzadeh, Z.; Lourenço, L.; Barros, J. Recycled steel fibre reinforced concrete failing in bending and in shear. *Constr. Build. Mater.* **2015**, *85*, 195–207. [CrossRef]
24. Lourenço, L.; Zamanzadeh, Z.; Barros, J.A.O.; Razazadeh, M. Shear strengthening of RC beams with thin panels of mortar reinforced with recycled steel fibres. *J. Clean. Prod.* **2018**, *194*, 112–126. [CrossRef]
25. Onuaguluchi, O.; Banthia, N. Scrap tire steel fiber as a substitute for commercial steel fiber in cement mortar: Engineering properties and cost-benefit analyses. *Resour. Conserv. Recycl.* **2018**, *134*, 248–256. [CrossRef]
26. Centonze, G.; Leone, M.; Aiello, M.A. Steel fibers from waste tires as reinforcement in concrete: A mechanical characterization. *Constr. Build. Mater.* **2012**, *36*, 46–57. [CrossRef]

27. Tlemat, H.; Pilakoutas, K.; Neocleous, K. Stress-strain characteristic of SFRC using recycled fibres. *Mater. Struct.* **2006**, *39*, 365–377. [CrossRef]
28. Neocleous, K.; Tlemat, H.; Pilakoutas, K. Design issues for concrete reinforced with steel fibers, including fibers recovered from used tires. *ASCE J. Mater. Civ. Eng.* **2006**, *18*, 677–685. [CrossRef]
29. Vandewalle, L.; Dupont, D. Bending Test and Interpretation. Test and design methods for steel fibre reinforced concrete—Background and experiences. In Proceedings of the RILEM TC 162-TDF Workshop, Bochum, Germany, 20–21 March 2003; RILEM Publications, S.A.R.L., Schnütgen, B., Vandevalle, L., Eds.;
30. Abrishambaf, A. Creep Behaviour of Cracked Steel Fibre Reinforced Self-Compacting Concrete Laminar Structures. Ph.D. Thesis, Department of Civil Engineering, School of Engineering of the University of Minho, Guimarães, Portugal, 2015.
31. Salehian, H.; Barros, J.A.O.; Taheri, M. Evaluation of the influence of post-cracking response of steel fibre reinforced concrete (SFRC) on load carrying capacity of SFRC panels. *Constr. Build. Mater.* **2014**, *73*, 289–304. [CrossRef]
32. Solgaard, A.O.S.; Küter, A.; Edvardsen, C.; Stang, H.; Geiker, M. Durability aspects of steel fibre reinforced concrete in civil infrastructure. In Proceedings of the 2nd International Symposium on Service Life Design for Infrastructure, Delft, The Netherlands, 4–6 October 2010.
33. Barros, J.; Pereira, E.; Santos, S. Lightweight panels of steel fibre reinforced self-compacting concrete. *J. Mater. Civ. Eng.* **2007**, *19*, 295–304. [CrossRef]
34. Soltanzadeh, F.; Barros, J.A.O.; Santos, R.F.C. High performance fiber reinforced concrete for the shear reinforcement: Experimental and numerical research. *Constr. Build. Mater.* **2015**, *77*, 94–109. [CrossRef]
35. di Prisco, M.; Ferrara, L.; Lamperti, M.G.L. Double edge wedge splitting (DEWS): An indirect tension test to identify post-cracking behaviour of fiber reinforced cementitious composites. *Mater. Struct.* **2013**, *46*, 1893–1918. [CrossRef]
36. ASTM C1550-08. *Standard Test Method for Flexural Toughness of Fiber Reinforced Concrete (Using Centrally Loaded Round Panel)*; ASTM International: West Conshohocken, PA, USA, 2008.
37. Minelli, F.; Plizzari, G.A. Fiber reinforced concrete characterization through round panel test—Part I: Experimental study. In Proceedings of the Fracture Mechanics of Concrete and Concrete Structures (FraMCOS-7)—High Performance, Fiber Reinforced Concrete, Special Loadings and Structural Applications, Jeju, Korea, 23–28 May 2010; Korea Concrete Institute, Oh, B.H., Chol, C.O., Lan, C., Eds.;
38. Lameiras, R.; Barros, J.A.O.; Azenha, M. Influence of casting condition on the anisotropy of the fracture properties of Steel Fibre Reinforced Self-Compacting Concrete (SFRSCC). *Cement Concrete Compos.* **2015**, *59*, 60–76. [CrossRef]
39. Abrishambaf, A.; Cunha, V.M.C.F.; Barros, J.A.O. The influence of fibre orientation on the post-cracking tensile behaviour of steel fibre reinforced self-compacting concrete. *Fract. Struct. Integr.* **2015**, *31*, 38–53. [CrossRef]
40. Abrishambaf, A.; Barros, J.A.O.; Cunha, V.M.C.F. Tensile stress-crack width law for steel fibre reinforced self-compacting concrete obtained from indirect (splitting) tensile tests. *Cement Concrete Compos.* **2015**, *57*, 153–165. [CrossRef]
41. Cunha, V.M.C.F. Steel Fibre Reinforced Self-Compacting Concrete (from Micro-Mechanics to Composite Behaviour). Ph.D. Thesis, Department of Civil Engineering, School of Engineering of the University of Minho, Guimarães, Portugal, 2010.
42. Eberhardt, C.; Clarke, A. Fibre-orientation measurement in short-glass-fibre composites. Part I: Automated, high-angular-resolution measurement by confocal microscopy. *Compos. Sci. Technol.* **2001**, *61*, 1389–1400. [CrossRef]
43. Soroushian, P.; Lee, C.D. Distribution and orientation of fibers in steel fiber reinforced concrete. *ACI Mater. J.* **1990**, *87*, 433–439.
44. NT BUILD 492. *Concrete, Mortar, and cEment-Based Repair Materials: Chloride Migration Coefficient from Non-Steady-State Migration Experiments*; NORDTEST: Espoo, Finland, 1999.
45. ASTM C1556-03. *Standard Test Method for Determining the Apparent Chloride Diffusion Coefficient of Cementitious Mixtures by Bulk Diffusion*; ASTM International: West Conshohocken, PA, USA, 2003.
46. NT BUILD 443. *Concrete, Hardened: Accelerated Chloride Penetration*; NORDTEST: Espoo, Finland, 1995.

47. Frederiksen, J.M.; Mejlbro, L.; Nilsson, L.-O. *Fick's 2nd Law—Complete Solutions for Chloride Ingress into Concrete—with Focus on Time Dependent Diffusivity and Boundary Condition*; Report TVBM-3146; Lund University, Institute of Technology, Division of Building Materials: Lund, Sweden, 2008; 110p.
48. Yang, C.-C.; Liang, C.-H. A modified colorimetric method to determine the chloride profile from the ponding test. *J. Chin. Inst. Eng.* **2014**, *37*, 419–427. [CrossRef]
49. Tang, L. Electrically accelerated methods for determining chloride diffusivity in concrete-current development. *Mag. Concrete Res.* **1996**, *48*, 173–179. [CrossRef]
50. Lay, S.; Liebl, S.; Hilbig, H.; Schieβl, P. New method to measure the rapid chloride migration coefficient of chloride-contaminated concrete. *Cement Concrete Res.* **2004**, *34*, 421–427. [CrossRef]
51. Bogas, J. Characterization of structural concretes with lightweight expanded clay aggregates. Ph.D. Thesis, Department of Civil Engineering, Technical University of Lisbon, Lisbon, Portugal, 2011. (In Portuguese).
52. Poulsen, E.; Mejlbro, L. *Diffusion of Chloride in Concrete: Theory and Application (Modern Concrete Technology)*, 1st ed.; Taylor & Francis: London, UK; New York, NY, USA, 2006.
53. Tang, L.; Sørensen, H.E. Precision of the Nodic test methods for measuring chloride transport diffusion/migration coefficients. *Mater. Struct.* **2001**, *34*, 479–485. [CrossRef]
54. Yuan, Q.; De Schutter, G.; Shi, C.; Audenaert, K. The relationship between chloride diffusion and migration coefficients in concrete. In Proceedings of the 1st International Conference on Microstructure Related Durability of Cementitious Composites, Nanjing, China, 13–15 October 2008; pp. 553–563.
55. Otsuki, N.; Nagataki, S.; Nakashita, K. Evaluation of $AgNO_3$ solution spray method for measurement of chloride penetration into hardened cementitious matrix materials. *ACI Mater. J.* **1992**, *89*, 587–592. [CrossRef]
56. Chiang, C.T.; Yang, C.C. Relation between the diffusion characteristic of concrete from salt ponding test and accelerated chloride migration test. *Mater. Chem. Phys.* **2007**, *106*, 240–246. [CrossRef]
57. Alonso, C.; Andrade, C.; Castellote, M.; Castro, P. Chloride threshold values to depassivate reinforcing bars embedded in a standardized OPC mortar. *Cement Concrete Res.* **2000**, *30*, 1047–1055. [CrossRef]
58. Berrocal, C.; Lundgren, K.; Löfgren, I. Influence of steel fibres on corrosion of reinforcement in concrete in chloride environments: A review. In Proceedings of the International Conference: FC2013-Fiber Concrete 2013, Prague, Czech Republic, 12–13 September 2013.
59. Janotka, I.; Krajcí, L.; Komlos, K.; Frtalová, D. Chloride corrosion of steel fibre reinforcement in cement mortar. *Int. J. Cement Compos. Lightweight Concrete* **1989**, *11*, 221–228. [CrossRef]
60. Song, L.; Sun, W.; Gao, J. Time dependent chloride diffusion coefficient in concrete. *J. Wuhan Univ. Technol. Mater. Sci. Ed.* **2013**, *28*, 314–319. [CrossRef]